INT. J. ELECTRONICS, 1966, VOL. 20, NO. 6, 583–599

Electrical Transport in *n*Ge–*p*GaAs Heterojunctions†

By A. R. RIBEN‡ and D. L. FEUCHT

Electrical Engineering Department, Carnegie Institute of Technology, Pittsburgh, Pennsylvania

[Received April 22, 1966]

ABSTRACT

A multi-step recombination-tunnelling model, similar to that used to describe the excess current in tunnel diodes, is developed to explain the observed electrical characteristics of *n*Ge–*p*GaAs heterodiodes. Two different, but quite similar models are used to qualitatively describe the observed forward and reverse characteristics. Quantitative agreement with the experimental characteristics of the many devices presented is obtained by an empirical modification of the resulting equations. The lack of minority carrier injection in these devices is in agreement with the proposed model.

§ 1. INTRODUCTION

IN a previous paper the authors (Riben and Feucht 1966) showed that the functional behaviour of the forward characteristics of a *n*Ge–*p*GaAs heterojunction could be explained on the basis of band-to-band tunnelling coupled with recombination processes. Similarly the functional behaviour in the reverse direction could be obtained from a Zener tunnelling model. The forward current density was expressed as:

$$J_f = BN_t \exp\left[-\alpha(V_d - K_2 V_a)\right], \tag{1}$$

where B is a constant, N_t is the density of traps per cubic centimetre, V_d is the diffusion voltage, $K_2 V_a$ is the voltage drop on the GaAs side of the junction, and $\alpha = 8\pi(2m^* q)^{1/2}(3\hbar H)^{-1}$, where m^* is the electron effective mass in the forbidden region, q is the electronic charge, h is Planck's constant and H is a constant.

The reverse current density was given as:

$$J_r = (-8q^2 V_a)(ha^2)^{-1} \exp\left[-\alpha(E_{g_1} + \Delta E_v)^{1/2}(V_d - V_a)^{-1/2}\right], \tag{2}$$

where E_{g_1} is the energy gap of germanium, ΔE_v is the difference in electron affinity for the valence band, a is the GaAs lattice constant and the other symbols are as defined above. In this work experimental characteristics

† Communicated by the Authors. This work is a portion of a thesis submitted by A. R. Riben in partial fulfilment of the requirements for the degree of Doctor of Philosophy at the Carnegie Institute of Technology. Support for this work was provided in part by the U.S. Army Research Office (Durham) Contract DA-31-124-ARO(D)-131.

‡ Present Address: Hamilton Standard, Electronics Department, Broadbrook, Connecticut.

of these devices are discussed in more detail. Certain modifications to the previous tunnelling models are presented which result in a better fit between theory and experiment. The results of this work are then related to the use of heterojunctions as wide band gap emitters.

§ 2. Device Fabrication

The devices were made from junctions grown by means of the germanium di-iodide disproportionation reaction (discussed by Ruth *et al.* 1960), at 400°C, with two exceptions. In order to eliminate the iodide process itself as a contributor to the electrical properties, junctions were grown by means of a solution growth technique (Nelson 1963, Riben 1965) and a close-spaced chloride reaction (Nicoll 1963, Riben 1965). These devices in general had the same characteristics as those made by the iodide process. Several different methods were used to prepare the substrates prior to growth, cleaving *in situ*, chemical etching and iodine etching. A correlation between the type of surface preparation and the grown layer quality as well as the overall electrical behaviour of the devices has been discussed in a paper by Riben *et al.* (1966).

The devices were fabricated by etching a mesa in the grown germanium layer, and thermal compression bonding two gold leads to the mesa. The gallium arsenide side of the device was soldered to a gold-plated kovar header. This three-lead structure allowed elimination of the contact resistance of the bonded lead (normally 50 to 100 ohms). In this way it was possible to very nearly measure the true junction voltage (the voltage dropped across the bulk semiconductor could normally be neglected).

§ 3. Experimental Results

3.1. *Forward Characteristics*

Figures 1 and 2 show the forward current–voltage characteristics and the forward current–temperature characteristics for a diode made by growing germanium on a cleaved gallium arsenide seed (110 plane); and also a diode grown at the same time on an iodine-etched (111As plane) seed of the same material. The dopings were $1{\cdot}5 \times 10^{18}$ donors/cm^{-3} (measured by the four-point probe method) for the germanium, and $1{\cdot}77 \times 10^{17}$ acceptors cm^{-3} (obtained by capacitance measurements) for the GaAs.

Immediately evident from fig. 1 is the fact that as the orientation and the surface preparation are changed, the current density changes; however, the slopes of the curves are not significantly different. Since the number of dislocations in a germanium arsenide seed layer grown on an iodine-etched germanium seed is larger by a factor of 30 than for a layer grown on a cleaved germanium seed (Riben 1965 and Riben *et al.* 1966), it is reasonable to assume that this order of magnitude change occurs for similar changes in the gallium arsenide seed preparation. This could account for an increase in the density of band-gap states, which in turn would account for an increase in current density in accordance with eqn. (1). On the other hand, a change in orientation may facilitate tunnelling by changing

Fig. 1

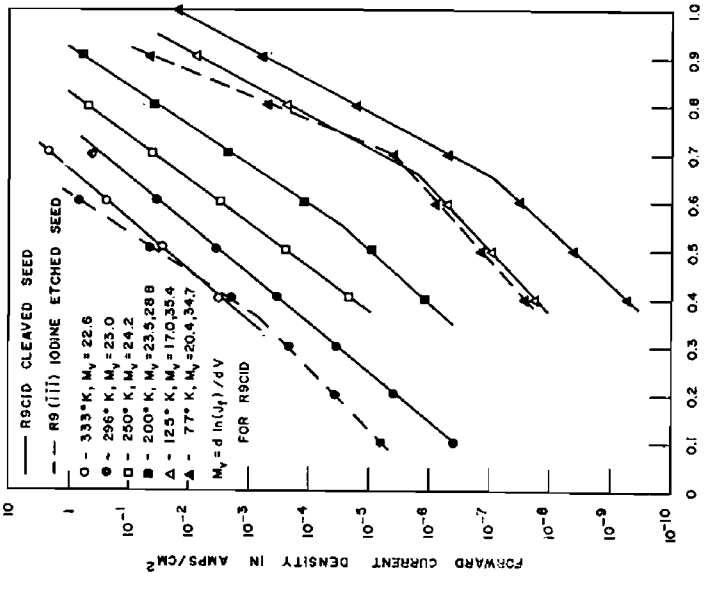

Forward current–voltage characteristics for two nGe–pGaAs heterodiodes at several temperatures, RCID and R9(111).

Fig. 2

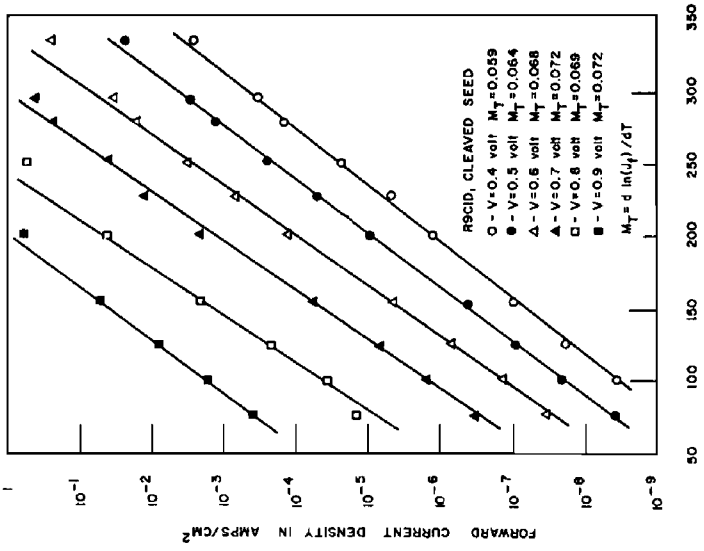

Forward current–temperature characteristics of a nGe–pGaAs heterodiode (R9CID) for several values of voltage.

the phonon field and in this way increase the tunnelling probability and the current density. A change in the barrier with orientation is also possible (Fang and Howard 1964), but capacitance measurements on the R9 ($\overline{111}$) diode showed that the same built-in diffusion voltage was present, and therefore the barrier was the same for the (110) plane and the (111)As plane. Looking at fig. 2 which shows the behaviour of the logarithm of the forward current as a function of temperature for constant bias, it can be seen that it varies linearly with temperature and that the slope of the resulting line is a function of voltage.

Fig. 3

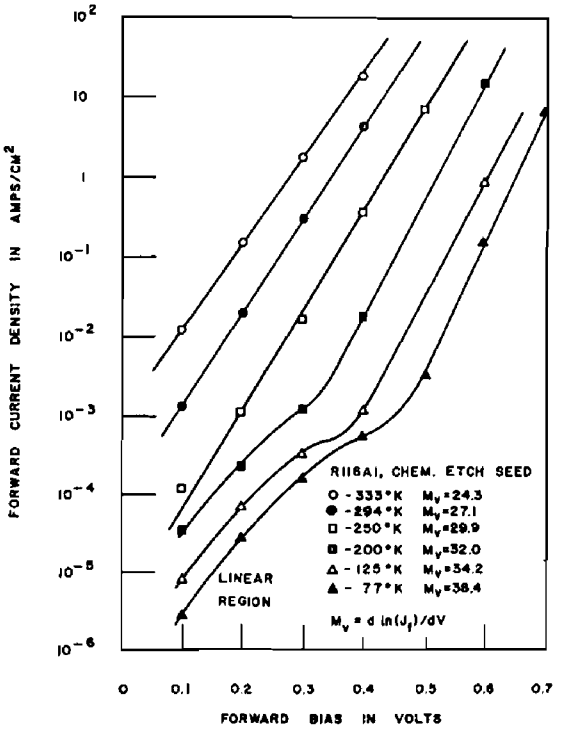

Forward current–voltage characteristics of a *n*Ge–*p*GaAs heterojunction (R116A1) at several temperatures.

Figures 3 and 4 show the forward current–voltage and current–temperature characteristics respectively for a second heterodiode made by growing germanium on non-degenerate gallium arsenide. For this diode, the germanium has a doping of 4×10^{17} donors cm^{-3} and was grown on a chemically etched gallium arsenide seed which the supplier specified had a doping of 10^{18} acceptors cm^{-3}. Here again the characteristics are seen to be very similar to those of an R9 diode (figs. 1 and 2). The curved region at low temperatures shown in fig. 3 is a linear variation of the current with applied voltage, which has been reduced to some extent by etching the device in white etch ($5HNO_3$, 1HF), and is probably due to surface leakage.

The temperature characteristic of this R116A1 diode at constant voltage has two slopes for voltages less than 0·6 volts. The large slope has almost the same value as that for the R9 diode, whereas the smaller slope corresponds to the temperature dependence of the linear current region and has no meaning in a comparison of the temperature dependences of the expotential currents in these devices. Even though the dopings are quite different in these diodes compared to the R9 diodes, the functional

Fig. 4

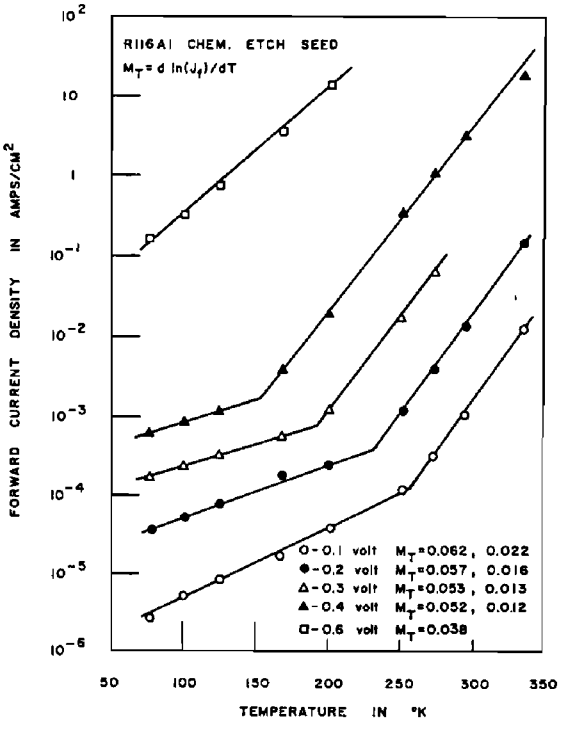

Forward current–temperature characteristics of a *n*Ge–*p*GaAs heterojunction (R116A1) for several values of voltage.

characteristics of the forward currents are the same. In general, the forward current for all *n*Ge–*p*GaAs heterodiodes investigated could be expressed by the empirical equation (for forward bias larger than a few kT):

$$J_f = J_0 \exp(\beta T + \gamma V_a), \tag{3}$$

where β and γ are functions of voltage and temperature respectively and J_0 is the current magnitude at 296°K. The slopes of the logarithm of this current with respect to voltage and temperature are given by:

$$M_V = \left.\frac{d \ln J_f}{dV_a}\right|_{T=\text{const}} = \gamma + T\frac{\partial \beta}{\partial V_a} \tag{4}$$

and

$$M_T = \left.\frac{d \ln J_f}{dT}\right|_{V_c=\text{const}} = \beta + V_a \frac{\partial \gamma}{\partial T}. \tag{5}$$

Table 1. Summary of data for several forward biased *n*Ge–*p*GaAs heterojunctions

Diode	Type†	Ge doping donors/cm³	GaAs doping acceptors/cm³	M_V‡ (296°K)	J_0 amps/cm²	M_T (0·4 v)	V_d§ (v)	E_V (ev)
R9C1D	1	$1{\cdot}5\times10^{18}$	$1{\cdot}77\times10^{17}$	23	$3{\cdot}4\times10^{-8}$	$5{\cdot}8\times10^{-2}$	1·06	0·56
R9($\overline{111}$)	5	$1{\cdot}5\times10^{18}$	$1{\cdot}77\times10^{17}$	17·7–25·5	$1{\cdot}1\times10^{-6}$	$6{\cdot}8\times10^{-2}$	1·06	0·56
R9(111)	6	$1{\cdot}5\times10^{18}$	$1{\cdot}77\times10^{17}$	25·5	$7{\cdot}6\times10^{-7}$	$6{\cdot}4\times10^{-2}$	0·89	0·39
R58PB	4	4×10^{17}	$1{\cdot}77\times10^{17}$	16·5–29·5	$7{\cdot}75\times10^{-6}$	$4{\cdot}9\times10^{-2}$	1·04	0·56
R59($\overline{111}$)A	7	4×10^{17}	$1{\cdot}77\times10^{17}$	20·6	$4{\cdot}25\times10^{-5}$	$3{\cdot}4\times10^{-2}$	1·01	0·53
R59(110)C	4	4×10^{17}	$1{\cdot}77\times10^{17}$	32·9	$8{\cdot}1\times10^{-9}$	—	1·03	0·55
R116A1	7	4×10^{17}	10^{18}	27·1	$8{\cdot}45\times10^{-5}$	$5{\cdot}2\times10^{-2}$	—	—
R116B1	7	4×10^{17}	10^{19}	25·3	$3{\cdot}5\times10^{-2}$	—	—	—
R113C1	1	10^{19}	$2{\cdot}25\times10^{17}$	13·2–26·9	$5{\cdot}5\times10^{-5}$	$4{\cdot}9\times10^{-2}$	1·08	0·51
R133C1b4	2	10^{19}	$2{\cdot}25\times10^{17}$	15·2–26·9	$1{\cdot}2\times10^{-4}$	—	1·08	0·51
R133C1E	3	10^{19}	$2{\cdot}25\times10^{17}$	12·4–26·9	8×10^{-4}	—	1·08	0·51
R133($\overline{111}$)E	5	10^{19}	$2{\cdot}25\times10^{17}$	54·5	8×10^{-4}	$5{\cdot}0\times10^{-2}$	—	—
L6C	8	—	$2{\cdot}25\times10^{17}$	36·6	$2{\cdot}3\times10^{-6}$	$4{\cdot}2\times10^{-2}$	0·75	—
11–2–3L	9	10^{19}	10^{18}	21·5	$1{\cdot}57\times10^{-3}$	$2{\cdot}3\times10^{-2}$	—	—

† See table 2.

‡ When two values of M_V are given, it indicates a sharp break from one slope to another.

§ V_d was obtained from capacitance measurements.

$M_V = \partial \ln J_f/\partial V_a$; $M_T = \partial \ln J_f/\partial T$; $\Delta E_v = V_d + \delta_1 + \delta_2 - E_{g_1}$.

Table 1 gives a summary of the forward characteristics of several nGe–pGaAs heterojunctions in terms of J_0, M_V and M_T. Table 2 explains the type of growth process and seed preparation used to make these devices.

Table 2. Description of the growth parameters for the nGe–pGaAs heterojunctions listed in tables 1 and 3

Type	Growth plane	Growth process	Substrate preparation
1	110	Germanium di-iodide reaction	Seed cleaved during growth
2	110	Germanium di-iodide reaction	Seed cleaved in air
3	110	Germanium di-iodide reaction	Seed cleaved in air and chemically etched
4	110	Germanium di-iodide reaction	Seed lapped and chemically etched
5	111 arsenic face	Germanium di-iodide reaction	Seed lapped, chemically etched and iodine etched
6	111 gallium face	Germanium di-iodide reaction	Seed lapped, chemically etched and iodine etched
7	111 arsenic face	Germanium di-iodide reaction	Seed lapped and chemically etched
8	111 arsenic face	Close-spaced chloride reaction	Seed lapped and chemically etched
9	111 arsenic face	Solution growth technique	Seed lapped and chemically etched

It is evident from tables 1 and 2 that the slope of the $\ln(J_f)$ versus V_a curve, M_V, is relatively independent of doping, temperature (M_V changes by less than a factor of 2 for the temperature range 77°K to 296°K), and also the type of growth process, the surface preparation and the orientation. The set of R133 diodes, fabricated by growing Ge simultaneously on several GaAs seeds from the same ingot slice, shows a dependence of current magnitude on substrate surface preparation. Due to the scatter of the data of other devices, it is impossible to draw any conclusions on the effect of orientation or doping on the current magnitude. The current magnitude is strongly dependent on the number of band gap states which is most likely a function of orientation, doping and the particular growth run.

All diodes, whose capacitance could be measured, yielded values of V_d, the diffusion voltage, in a range such that they could be described by the equilibrium band diagram proposed by Anderson (1962). There was no significant change in V_d as the surface preparation was changed, and there was essentially no difference in the values of V_d, ΔE_v and ΔE_c for diodes orientated on either the (110) plane or the (111)As plane. In agreement with the work of Fang and Howard (1964), however, there was a decrease of approximately 0·2 ev in ΔE_v as the plane was changed from the (111)As to the (111)Ga plane. However, the electrical characteristics did not change to any extent.

The temperature dependence of the heterojunctions was also rather insensitive to doping, orientation or substrate surface preparation. In all cases (except R116B1 in which the GaAs was degenerate), the logarithm of the current was a linear function of temperature, and the slope of the line was a linear function of voltage. Also, at a given voltage, the slope of the $\ln(J_f)$ versus T curve, M_T, has nearly the same value for most of the devices.

Included in table 1 are the experimental parameters for two diodes made with the close-spaced chloride system L6C and by the solution growth technique, 11–6–3L. The characteristics of these devices are essentially the same as those made by the iodine process.

3.2. *Reverse Characteristics*

Figure 5 shows the log–log plot of the reverse current of the R9ClD diode as a function of voltage at several temperatures. For lower voltages ($-V_a < 0{\cdot}4$ v) the current is a linear function of the voltage while at higher voltages, the current is proportional to V^m where m is greater than 3 and is a function of temperature (Riben 1965). Figure 6 shows the current as a function of temperature for several values of voltage for the same diode. It is evident that $\ln(J_r)$ is a linear function of temperature, although there is some deviation at the higher values of temperature probably due to thermal excitation of carriers over the ΔE_v barrier.

It was shown in the previous paper that a power law function as given by eqn. (2) could be achieved over a range of voltage by use of a Zener tunnelling model. Therefore, it is advantageous to plot the $\ln(J/-V_a)$ as a function of $(V_d - V_a)^{-1/2}$ as shown in fig. 7 for the R9 diodes. The deviation from the expected straight line behaviour for $(V_d - V_a)^{-1/2} < 0{\cdot}35$ in fig. 7 is due to the onset of avalanche breakdown in the GaAs. The electric field in the GaAs at breakdown is 8×10^5 volts cm^{-1}, which is in good agreement with the value of 10^6 volts cm^{-1} given by Logan *et al.* (1962).

Figures 5, 6 and 7 are typical of all *n*Ge–*p*GaAs heterojunctions investigated, regardless of doping or growth process. The reverse current in the power law region can be described by the empirical formula given by:

$$J_r = -G_0 V_a \exp[-U(V_d - V_a)^{-1/2}], \tag{6}$$

where the parameter U is a function of temperature and G_0 is a constant. The slopes of the curves plotted in fig. 6 are given by:

$$\left.\frac{d\ln[J_r/-V_a]}{d(V_d - V_a)^{-1/2}}\right|_{T=\text{const.}} \equiv -U_V \tag{7}$$

and those in fig. 7 by:

$$\left.\frac{d\ln J_r}{dT}\right|_{V_a=\text{const}} = -(V_d - V_a)^{-1/2}\frac{\partial U}{\partial T} \equiv U_T. \tag{8}$$

Table 3 gives a summary of the reverse characteristics in terms of G_0, U_V and U_T. It appears that the parameters G_0, U_V and U_T are not simple functions of either doping, orientation, surface preparation or growth conditions.

Fig. 5

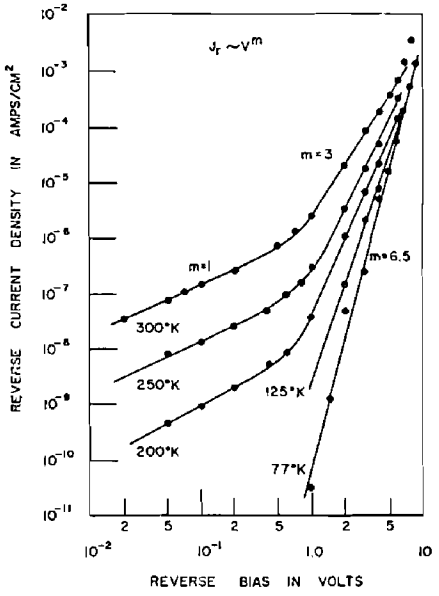

Reverse current–voltage characteristics for a *n*Ge–*p*GaAs heterodiode (R9C1D cleaved seed) at several temperatures.

Fig. 6

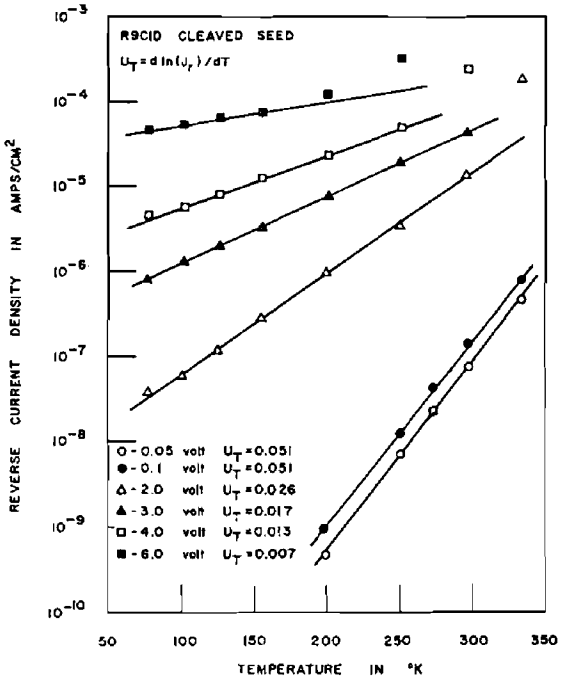

Reverse current–temperature characteristics of a *n*Ge–*p*GaAs heterojunction (R9C1D) for several values of voltage.

Fig. 7

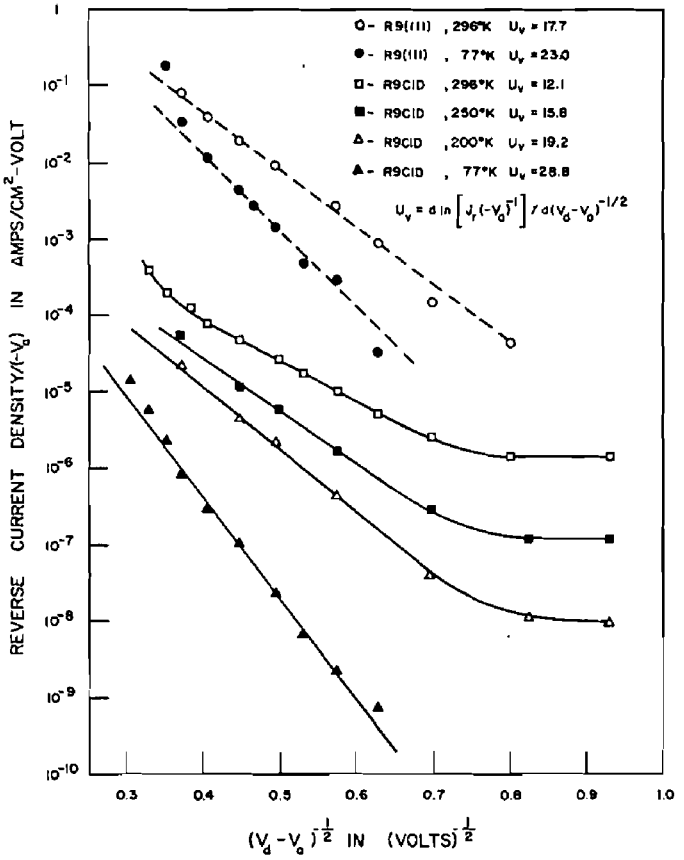

Reverse current–voltage characteristics of two nGe–pGaAs heterojunctions at several temperatures. (R9ClD cleaved seed and R9($\overline{1}\overline{1}\overline{1}$) I_2 etched seed.)

Table 3. Summary of data for several reverse biased nGe–pGaAs heterojunctions

Diode	Type†	G‡ (mho)/cm²	U_V (296°K)	U_T (bias)	V_d (v)
R9ClD	1	$1{\cdot}41\times10^{-6}$	−12·1	$1{\cdot}14\times10^{-2}$ (2 v)	1·06
R9($\overline{1}\overline{1}\overline{1}$)	5	$2{\cdot}22\times10^{-5}$	−23·0	$4{\cdot}5\times10^{-3}$ (2 v)	1·06
R9(111)	6	$4{\cdot}25\times10^{-5}$	−38·4	$3{\cdot}38\times10^{-3}$ (4 v)	0·89
R59PB	4	$2{\cdot}88\times10^{-4}$	−44·2	$3{\cdot}5\times10^{-3}$ (7 v)	1·04
R59($\overline{1}\overline{1}\overline{1}$)A	7	$1{\cdot}6\times10^{-4}$	−17·7	$5{\cdot}2\times10^{-3}$ (2 v)	1·01
R59(110)C	4	—	−16·9	6×10^{-3} (2 v)	1·03
R116A1	7	$3{\cdot}54\times10^{-3}$	−35·4	$1{\cdot}56\times10^{-3}$ (1 v)	1·0§
R116B1	7	1·4	−46	$6{\cdot}5\times10^{-3}$ (0·45 v)	1·0
R133C1	1	$1{\cdot}55\times10^{-3}$	−25·6	—	1·08
R133C1b4	2	$2{\cdot}7\times10^{-3}$	−20·9	—	1·08
R133C1E	3	$2{\cdot}2\times10^{-2}$	−1·68	—	1·08
L6C	8	$3{\cdot}9\times10^{-3}$	−24	—	0·75
11–2–3L	9	$6{\cdot}72\times10^{-2}$	−23	$2{\cdot}51\times10^{-3}$ (8 v)	1·1§

† See table 2.
‡ $G = J_r/V_a$ for $V_a \ll V_d$.
§ This value equals V_{d_0} and was found by curve fitting.
$U_V = \partial \ln [J_r(-V_a)^{-1}]/\partial(V_d - V_a)^{-1/2}$; $U_T = \partial \ln J_r/\partial T$.

§ 4. Development of the Multi-step Tunnelling Model

A comparison of the experimental results with eqns. (1) and (2) for the forward and reverse directions shows poor quantitative agreement between simple theory and experiment. In the following sections an attempt will be made to develop a multi-step recombination-tunnelling model, similar to that used to describe excess current in tunnel diodes, in order to explain the observed electrical characteristics.

4.1. *Forward Current Model*

In the forward direction, referring to figs. 1–4, there are several features of the characteristics which must be explained by the theory: the magnitude and temperature dependence of the slope of the $\log J_f$ versus V plot and the magnitude of the current†. Although the two parameters BN_t and α of eqn. (1) are unknown within limits and hence adjustable to some degree, it is impossible to obtain agreement on the points outlined above. In order to obtain agreement between theory and experiment at room temperature (297°K) for the R9CID diode (fig. 1) for example, α must equal 23 and $BN_t \simeq 10^3$. This value of α, however, requires an effective mass of $0{\cdot}007m_e$ for electrons traversing the forbidden region which seems unrealistically small.

The fact that we obtained such a small value of m^* is not too surprising, however, as most of the diodes studied did not have degenerate gallium arsenide. In this case the physical distance that the electron is required to tunnel in going from the germanium conduction band to the gallium arsenide valence band is very large (> 1000 Å) so that the expected tunnel current based on a value of $m^* = 0{\cdot}12m_e$ (the light hole mass in GaAs) is much smaller than observed. If the staircase path, such as is shown in fig. 8 (*a*), is assumed to be the actual tunnelling path, the tunnelling probability is modified and the resultant current equation will be different. Franz (1956) gives the tunnelling probability for an electron tunnelling from an impurity level into the conduction band as:

$$P = \exp[-4(2m^*)^{1/2}q^{1/2}E_t^{3/2}/3\hbar F], \tag{9}$$

where E_t is the energy level of the trap below the conduction band edge and F is the electric field in the depletion region on the GaAs side of the junction. Assuming that this equation holds for tunnelling between trap levels, and assuming that the traps are uniformly spaced in energy, the current can be described by:

$$J_f = \beta N_t \exp[-\alpha R E_t^{3/2}/(V_d - V_a)^{1/2}], \tag{10}$$

where R, the number of steps required to traverse the depletion region, is given by:

$$R = (V_d - K_2 V_a) E_t^{-1}. \tag{11}$$

† The sharp break in the J versus V curves (fig. 1) exhibited by most diodes will be considered later.

The current is then given by:

$$J_t = \beta N_t \exp\left[-\alpha E_t^{1/2}(V_d - K_2 V_a)(V_d - V_a)^{-1/2}\right]. \quad (12)$$

E_t must be proportional to the square of the electric field, i.e. $E_t = \theta(V_d - V_a)$ in order for this equation to agree functionally with the experimental data. Since E_t is a type of average barrier due to the close spacing of the energy levels in the forbidden region, it appears reasonable that, as the field changes, the dominant barrier heights will change. This is due to the fact that if there are levels available, and the electron cannot penetrate far

Fig. 8

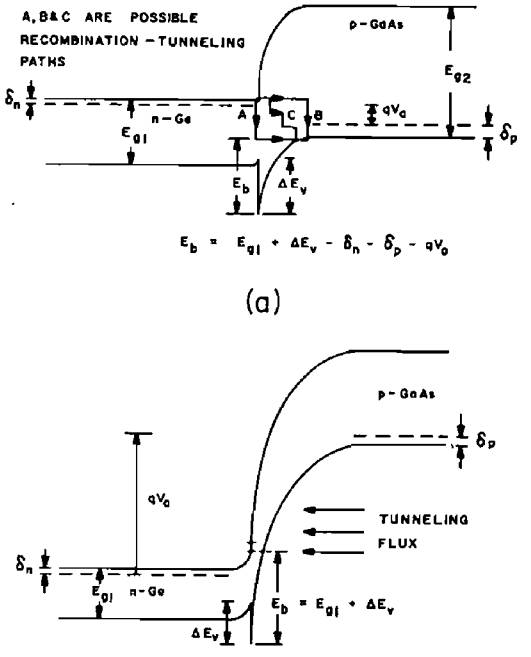

Proposed tunnelling models for the *n*Ge–*p*GaAs heterojunction, (*a*) forward bias, (*b*) reverse bias.

enough to reach a certain level, it can tunnel into a level which is not quite as deep. Thus the effective barrier is lower than that for a higher field. It is not clear what the relation between the field and the barrier height should be, but $E_t = \theta(V_d - V_a)$ was chosen to obtain functional agreement between theory and experiment. This assumption of a field-dependent barrier leads to an M_V which is independent of the gallium arsenide doping as seen in table 1.

Using the above empirical relation for E_t, the forward current density is given as:

$$J_t = \beta N_t \exp\left[-\alpha\theta^{\frac{1}{2}}(V_d - K_2 V_a)\right]. \quad (13)$$

M_V, the derivative of $\ln(J_f)$ with respect to V_a, at a constant temperature, is then equal to $\alpha K_2 \theta^{1/2}$ which has a similar value for most of the diodes in table 1. For the R9C1D diode assuming a value of $0{\cdot}12m_e$ again for m^*, θ approximately equals 0·058 and the number of steps R,

$$\{R = (V_d - K_2 V_a)/\theta(V_d - V_a)\},$$

required for this tunnelling model is 17, but it is directly proportional to the value assumed for m^*. The number of steps required to obtain quantitative agreement between experiment and theory varied, depending on the doping and surface preparation of the diodes. For example, only three steps are required for the R116A1 diode shown in fig. 3 assuming an m^* of $0{\cdot}12m_e$.

Fig. 9

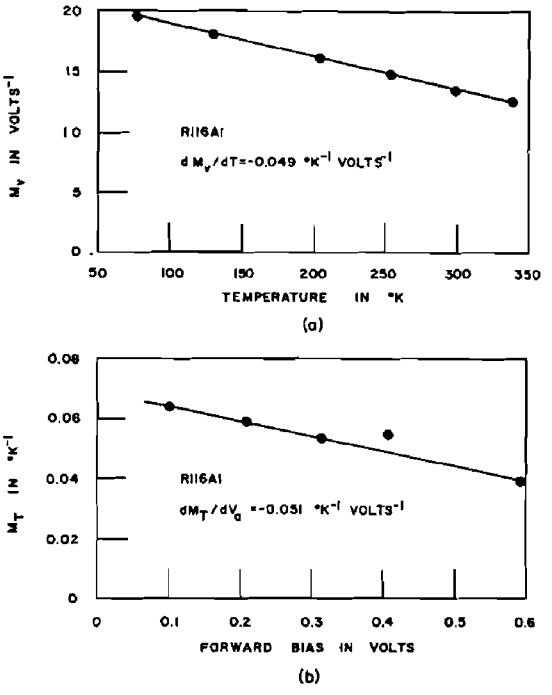

The parameters (*a*) M_V and (*b*) M_T as a function of temperature for diode R116A1.

M_V, as shown in fig. 9 (*a*) for R116A1 decreases linearly as the temperature is increased over a temperature range from 77°c to 330°c. $M_V = M_0 - \lambda_m T$, for most diodes with the slope $\lambda_m = -dM_V/dT$ approximately equal to 5×10^{-2}. This variation with temperature would be explained by a linear variation of $\theta^{1/2}$ with temperature†. This does not seem unreasonable as the variation of the band gap with temperature is approximately linear over this temperature range.

† Since the variation of $\theta^{1/2}$ with temperature is small over this range θ varies approximately linearly with temperature.

Using the temperature dependence for $\theta^{1/2}$ from above and assuming V_d to vary linearly with temperature† ($V_d = V_{d_0} - \lambda_d T$), the derivative of $\ln(J_f)$ with respect to temperature at a constant V_a, M_t is equal to $M_T = \lambda_m(V_d - K_2 V_a) K_2^{-1} + \alpha\theta^{1/2}\lambda_d$. The values of M_T which are independent of temperature are very similar for all the diodes and are given in table 1. M_T, as shown in fig. 9 (*b*), decreases linearly as the forward bias is increased from 0·1 to 0·6 volts as would be expected from the above equation. The slope of this curve dM_T/dV_a equals $-\lambda_m$ also, in agreement with the theory.

The sharp break in the $\log J_f$ versus V curves of fig. 1 indicates that the distribution of band gap states is not uniform as assumed in the above analysis. Some additional modification of eqn. (13) would be required to account for this break but it is not clear from the data what form this should take. Another mechanism that might exist, and has not been included in the model, is that of phonon-assisted tunnelling. This is expected because crystal momentum must be conserved as the electron tunnels from a (111) minima in the germanium conduction band to a (000) minima in the gallium arsenide valence band. This effect might be responsible for the changes in current magnitude as a function of crystal orientation that were seen in the R59 diodes.

It seems clear, based on the experimental evidence obtained, that a tunnel diode excess current model may be used to describe the forward current in a *n*Ge–*p*GaAs heterojunction. It should be noted that, although this work pertained to *n*Ge–*p*GaAs heterodiodes, a similar model will describe the behaviour of *n*Ge–*p*Si diodes made by both the iodine process and the solution growth process and 'Ge'–Si diodes made by an alloy technique described by Shewchun and Wei (1964).

4.2. *Reverse Current Model*

It was shown by the authors (Riben and Feucht 1966) in a previous paper that the power law region of the reverse current could qualitatively be explained by means of a Zener tunnelling model. The resulting current–voltage relation is given by eqn. (2). If, however, we compare the calculated value of the slope U of this characteristic, $U_r = -\alpha^{1/2}(E_{g1} + \Delta E_v)^{3/2}$, to the data of a typical diode such as R9C1D the calculated value is 137 (based on a value of $0{\cdot}12m_e$ for m^*), whereas the measured value of U_r is 14. As in the forward direction, a multi-step tunnelling mechanism, via states in the forbidden energy region of the GaAs, will give better agreement between theory and experiment.

Using the model fig. 8 (*b*), assuming the band gap states exist and applying the work of Franz (1956) for impurity tunnelling, the reverse

† $V_d = E_{g_1} + \Delta E_v - \delta_1 - \delta_2$, where $\delta_1 = kT \ln N_{c_1}/N_{d_1}$ and $\delta_2 = kT \ln N_{v_2}/N_{d_2}$. For a linear variation in band gap and ΔE_v, assuming $\ln N_{c_1}/N_{d_1}$ and $\ln N_{v_2}/N_{d_2}$ are independent of temperature, V_d varies linearly with temperature. Both of these assumptions are quite reasonable for the temperature ranges considered.

current can be expressed as:

$$J_r = (-q^2 a N_t V_a h^{-1}) \exp[-\alpha W E_r^{3/2}(V_d - V_a)^{-1/2}], \tag{14}$$

where E_r is the tunnelling barrier for each step, W is the number of steps required to traverse the entire energy barrier (i.e. $W = (E_{g_1} + \Delta E_v)/E_r$) and N_t is the density of available states in the depletion region. Using this expression for W, eqn. (14) may be written as:

$$J_r = (-q^2 a N_t V_a h^{-1}) \exp[-\alpha E_r^{1/2}(E_{g_1} + \Delta E_v)(V_d - V_a)^{-1/2}]. \tag{15}$$

The value of E_r required for agreement with the experimental data is 0·01 ev and the number of steps required is approximately 120 assuming a value of $0{\cdot}12 m_e$ for m^*.

Assuming that the change in the band gap of each of the materials is linear with temperature for the range 296°K to 77°K and that $E_r^{1/2} = E_{r_0}^{1/2} - \lambda_r T$, the rate of change of U_V†, $U_V = -\alpha E_r^{1/2}(E_{g_1} + \Delta E_v)$, with temperature is:

$$\frac{\partial U}{\partial T} = \alpha E_r^{1/2} \lambda_2 + (E_{g_1} + \Delta E_v)\lambda_r. \tag{16}$$

The value of λ_r necessary to obtain agreement with the experimental data for the R9ClD diode is approximately 2×10^{-4} ev °K^{-1}. Using the above approximations it can be shown that J_r varies linearly with temperature and $d \ln J_r/dT$ is a function of the applied voltage. This is an agreement with the experimental results (see fig. 6).

An approximation to the number of traps required can also be obtained since the magnitude $JV_a^{-1} \exp[U(V_d - V_a)^{1/2}]$ is given by $q^2 a N_t h^{-1}$. Using a value of 5·67 Å for a, the value of N_t for the R9ClD diode was found to be $5{\cdot}2 \times 10^7$ cm^{-3}. Although there was too much scatter in our data from device to device to arrive at any definite conclusions concerning the value of N_t, the number of traps required for any device was reasonable from the standpoint of the ability of the crystal to contain these defects.

As in the forward bias direction, in order to obtain quantitative agreement with the observed characteristics, the average barrier E_2 must be a function of the electric field. This does not seem unreasonable, but the required functional variation is quite complex and does not have a simple physical explanation.

Although the Zener tunnelling model does not predict any tunnelling current until enough bias is applied to align the electrons in the gallium arsenide valence band with the empty states in the germanium conduction band, the experiments (fig. 5) yield a current which is proportional to voltage for small voltages. This does not seem to be a surface current since surface preparation does not affect the magnitude of the observed current and the current is proportional to the area of the mesa

† $E_{v_1} = E_{1_0} - \lambda_1 T$ and $E_{v_2} = E_{2_0} - \lambda_2 T$, where 1 and 2 refer to the germanium and gallium arsenide respectively. $E_r^{1/2}$ would be expected to have the same type of temperature dependence as $E_t^{1/2}$, as it is a similar type of barrier approximation.

rather than its perimeter. A tunnelling process via a staircase path from the gallium arsenide valence band through the depletion region to the germanium conduction band functionally agrees with the observed low voltage characteristic. Even though the states are probably closely spaced, this would require the electrons to gain energy from the lattice by thermal excitation in order to traverse the path. This would lead to a small degree of junction cooling which would be difficult to detect and hence has not been verified.

§ 5. Discussion

We have shown that for both the forward and reverse bias, the *n*Ge–*p*GaAs heterojunction (and others) can best be described by tunnelling models which involve multi-step tunnelling and trap recombination processes in the forbidden energy region of the energy bands. Although good quantitative comparisons between theory and experiment were not possible because of the lack of knowledge of the band gap states, it was shown qualitatively that the experimental data were functionally consistent, and quasi-empirical equations were obtained which describe the heterojunction characteristics. It was not our intention to imply in this work that the tunnelling currents replace the thermal currents of Anderson (1962) or of Perlman and Feucht (1962), but rather that they exist in addition to the thermal currents. However, because of the discontinuities in the energy bands of the two materials, a large barrier exists for the thermal carriers, and the tunnelling current is the dominant current.

It would be interesting to perform an experiment in which the heterojunctions are bombarded with high-energy electrons (of the order of 1 MeV), since, as in the tunnel diode work of Chynoweth *et al.* (1961) and Roth *et al.* (1963), an increase in the currents would be expected. Unfortunately, the equipment required for such an experiment was not available in our laboratory.

An important feature of the tunnelling model presented here is that it does not require minority carrier transport, so very little transistor gain (if any) would be expected in a *pnp* transistor, fabricated with a gallium arsenide emitter. The data did indicate that because of the relatively small value of the discontinuity in the conduction band, a *p*Ge–*n*GaAs heterojunction should probably be governed by the thermal currents, and that injection in this device was likely. However, the characteristics of a few of these diodes (*p*Ge grown in *n*GaAs by the solution growth technique) were investigated, and although the characteristic did seem to be due to thermal current, it appeared to be the recombination–generation current described by Sah *et al.* (1957). Injection studies were carred out as a check on these conclusions, and no wide band gap emitter structure showed transistor action while homojunction structures, fabricated in the same manner, did exhibit transistor action.

References

Anderson, R. L., 1962, *Solid State Electronics*, **5**, 341.

Chynoweth, A. G., Feldman, W. L., and Logan, R. A., 1961, *Phys. Rev.*, **121**, 684.

Fang, F. F., and Howard, W. E., 1964, *J. appl. Phys.*, **35**, 612.

Franz, W., 1956, *Handbuch der Physik* (Berlin: Springer-Verlag), Chap. 17, p. 155.

Logan, R. A., Chynoweth, A. G., and Cohen, B. G., 1962, *Phys. Rev.*, **128**, 2518.

Nelson, H., 1963, *R. C. A. Rev.*, **24**, 603.

Nicoll, F. H., 1963, *J. electrochem. Soc.*, **110**, 1165.

Perlman, S. S., and Feucht, D. L., 1962, *Solid State Electronics*, **1**, 911.

Riben, A. R., 1965, Thesis, Carnegie Institute of Technology, Pittsburgh, Pennsylvania.

Riben, A. R., and Feucht, D. L., 1966, *Solid State Electronics* (in the press).

Riben, A. R., Feucht, D. L., and Oldham, W., 1966, *J. electrochem. Soc.*, **113**, 245.

Roth, H., Bernard, W., Zelders, P., and Schmid, A. P., 1963, *J. appl. Phys.*, **34**, 669.

Ruth, R., Marinace, J., and Dunlap, W., 1960, *J. Appl. Phys.*, **31**, 995.

Sah, C. T., Noyce, R., and Shockley, W., 1957, *Proc. Inst. Radio Engrs, N.Y.* **45**, 1228.

Shewchun, J., and Wei, L. Y., 1964, *J. electrochem. Soc.*, **111**, 1145.